



仿酶制剂ZIF-8@Pt用于清除活性氧治疗类风湿关节炎的研究*

雷雪兰, 邱 邈, 杜方雪[△]

四川大学华西医院 超声医学科(成都 610041)

【摘要】 目的 构建具备清除活性氧(reactive oxygen species, ROS)能力的铂金属掺杂ZIF-8纳米仿酶制剂(ZIF-8@Pt)并探讨其对类风湿关节炎(rheumatoid arthritis, RA)的治疗效果。方法 通过原位还原的方式得到ZIF-8@Pt纳米制剂并进行表征和仿酶能力测试后,使用RAW264.7细胞,分未处理组(untreated, UT)、阳性对照组(lipopolysaccharide, LPS)及治疗组(ZIF-8@Pt)进行细胞实验,探讨其清除胞内ROS实现抗炎的能力。使用胶原诱导大鼠建立关节炎模型(collagen-induced arthritis, CIA),分健康对照组(UT)、阳性对照组(Control组,注射PBS)及治疗组(ZIF-8@Pt,注射ZIF-8@Pt溶液),对膝关节进行局部注射治疗,通过大体评分、影像学观察、炎症因子检测以及病理学评估等探讨其针对RA的治疗效果。结果 在体外实验中,细胞内ROS水平及LPS诱导的巨噬细胞M1型极化,ZIF-8@Pt组与LPS组相比,差异有统计学意义($P<0.05$);在体内实验中,针对CIA大鼠血清及关节局部的炎症因子水平的检测,如白细胞介素-1 β (interleukin-1 β , IL-1 β)、C-反应蛋白(C-reactive protein, CRP)、肿瘤坏死因子- α (tumor necrosis factor- α , TNF- α)、精氨酸酶-1(arginase-1, Arg-1),ZIF-8@Pt组与Control组相比,差异有统计学意义($P<0.05$)。病理学评估表明,与Control组相比,ZIF-8@Pt可缓解关节局部缺氧,抑制血管新生、破骨活动以及巨噬细胞M1型极化($P<0.05$)。结论 ZIF-8@Pt仿酶制剂能够通过清除活性氧ROS而抑制巨噬细胞炎症极化进而改善RA炎症环境。同时,其可改善关节腔缺氧环境,抑制血管新生及骨破坏,对RA具有良好的治疗效果。

【关键词】 纳米材料 仿酶制剂 类风湿关节炎 活性氧 抗炎治疗

ZIF-8@Pt Nanozyme Used for Scavenging Reactive Oxygen Species in the Treatment of Rheumatoid Arthritis LEI Xuelan, QIU li, DU Fangxue[△]. Department of Ultrasound, West China Hospital, Sichuan University, Chengdu 610041, China

[△] Corresponding author, E-mail: 1531442337@qq.com

【Abstract】 Objective To formulate a ZIF-8 nano mimetic enzyme conjugated with platinum metal (ZIF-8@Pt) that can scavenge reactive oxygen species (ROS) and to explore its potential applications in the treatment of rheumatoid arthritis (RA). **Methods** The ZIF-8@Pt nanozyme was created by *in situ* reduction. Characterization of the nanozyme was then performed and its ability to mimic enzymes was investigated. Cell experiments were conducted using RAW264.7 cells, which were divided into three groups, including the untreated group (UT), the positive control group receiving lipopolysaccharide (LPS), which was designated as the LPS group, and the ZIF-8@Pt group receiving ZIF-8@Pt and LPS treatment. The cell experiments were conducted to evaluate the anti-inflammatory properties of ZIF-8@Pt through scavenging intracellular ROS. On the other hand, a collagen-induced arthritis (CIA) model was induced in rats. Similar to the group designations in the cell experiments, the rats were assigned to three groups, including a healthy control group (the UT group), a positive control group receiving a local injection of PBS solution in the knee joint, which was referred to as the control group, and a treatment group receiving a local injection of ZIF-8@Pt solution in the knee joint, which was referred to as the ZIF-8@Pt group. General evaluation, imaging observation, assessment of inflammatory factors, and pathological evaluation were performed to assess the therapeutic efficacy of ZIF-8@Pt against RA. **Results** The *in vitro* experiment revealed significant difference in the levels of intracellular ROS and LPS-induced M1-type macrophage polarization between the LPS group and the ZIF-8@Pt group ($P<0.05$). The *in vivo* experiment showed that significant difference in the levels of inflammatory factors, including interleukin-1 β (IL-1 β), C-reactive protein (CRP), tumor necrosis factor- α (TNF- α), and arginase-1 (Arg-1) in the knee joints of the CIA rats between the LPS group and the ZIF-8@Pt group ($P<0.05$). Comparing the findings for the ZIF-8@Pt group and the control group, pathology assessment revealed that ZIF-8@Pt reduced local hypoxia and suppressed osteoclastic activity, neovascularization, and M1-type macrophage polarization ($P<0.05$). **Conclusion** The ZIF-8@Pt enzyme mimetic inhibits macrophage inflammatory polarization by ROS scavenging, thereby improving inflammation in RA. Furthermore, the ZIF-8@Pt nanozyme improves the hypoxic environment and inhibits angiogenesis and bone destruction, demonstrating promising therapeutic efficacy for RA.

【Key words】 Nanomaterials Nanozyme Rheumatoid arthritis Reactive oxygen species Anti-inflammatory treatment

* 四川省卫健委医学科技项目(No. 21PJ012)和四川省科技厅项目(No. 2022YFH0112)资助

[△] 通信作者, E-mail: 1531442337@qq.com

出版日期: 2024-07-20

类风湿关节炎(rheumatoid arthritis, RA)是一种慢性全身性自身免疫性疾病,主要累及关节,其基本病理特征包括滑膜增生^[1]、滑膜血管翳形成^[2]和免疫细胞浸润^[3]。滑膜增生主要由成纤维滑膜样细胞的异常肿瘤样增殖所致^[4]。这一病理生理改变将造成关节腔内大量活性氧(reactive oxygen species, ROS)产生并形成缺氧微环境。正常机体内ROS的产生与清除保持动态平衡^[5];当RA发生时,巨噬细胞炎性代谢增强,ROS于关节腔滑膜处富集^[6],协同趋化因子,进一步加重组织炎症反应^[7]。而缺氧微环境的形成会上调缺氧诱导因子-1 α (hypoxia-inducible factor alpha, HIF-1 α)的表达,进而促进滑膜血管翳形成^[8]。同时,免疫细胞激活及促炎因子作用将进一步导致炎症和关节破坏,促进RA发展^[9-11]。在RA发生时,巨噬细胞在ROS等效应因子刺激下向促炎表型—M1型极化,该表型巨噬细胞会持续分泌诸如肿瘤坏死因子- α (tumor necrosis factor- α , TNF- α)、白细胞介素-1 β (interleukin-1 β , IL-1 β)等炎症因子,进一步加重关节炎^[12]。

RA的治疗一直是临床的难点。目前的治疗方法包括非甾体抗炎药、糖皮质激素及包括生物制剂在内的多种抗风湿病药的药物治疗^[13]。药物长期使用可能发生耐药性、胃肠道不适及骨髓抑制等副作用,且生物制剂价格昂贵,同时可能增加肺结核患病及发生严重感染的风险^[14]。因此,寻找新的且更加安全的治疗方法具有重要的临床和社会价值。既往研究表明,通过使用天然的过氧化氢酶(catalase, CAT)等清除ROS相关介质可以有效缓解RA疾病进程,降低局部滑膜增生,抑制关节破坏^[10,15-16]。然而,天然酶存在稳定性差、易失活、难制备、难提纯、成本高以及酶活性单一等固有局限性,极大地阻碍了其抗RA治疗的应用;而研究表明,纳米仿酶制剂可以模拟上述天然酶的催化过程,清除病变局部高水平富集的ROS。它们同时还具有高稳定性、易制备、成本低等优点,被广泛用于多种疾病的抗炎治疗。因此,本研究设计制备一种具有高效催化性能的仿CAT酶活性纳米制剂以高效清除病变关节局部的ROS,有望为RA治疗提供新的方案。现报告如下。

1 材料与方法

1.1 材料

1.1.1 主要试剂及耗材

2-甲基咪唑、Zn(NO₃)₂·6H₂O、CTAB和PtCl₄均购自中国Aladdin公司;免疫级牛Ⅱ型胶原蛋白和弗氏不完全佐剂购自美国Chondrex; α -MEM培养基、胎牛血清、PBS、双抗等购自Gibco;脂多糖(lipopolysaccharide, LPS)购自

Solarbio; DCFH-DA探针购自碧云天;大鼠TNF- α 、Arg-1、IL-1 β 、CRP等指标的ELISA试剂盒均购自泉州市睿信生物科技有限公司;抗酒石酸磷酸酶(tartrate-resistant acid phosphatase, TRAP)染色试剂盒购自南京建成;Anti-CD206抗体购自CST; Anti-CD31和Anti-iNOS抗体购自Abcam; Anti-HIF-1 α 抗体购自Novus。小鼠RAW264.7巨噬细胞来自中国科学院细胞库。细胞培养箱(美国Thermo Fisher Scientific公司);倒置荧光显微镜(Ti2, Nikon);Cytoflex流式细胞分析仪(美国Bekman coulter公司);Vevo 3100小动物超声成像系统(日本fujifilm公司);Micro-CT(美国PerkinElmer公司)。

1.1.2 实验动物

健康成年雄性SD大鼠,鼠龄7~8周,购自北京华阜康生物科技股份有限公司。所有实验动物均饲养于四川大学生命科技园实验动物中心SPF级无菌饲养间,25℃恒温,湿度50%~60%,自由进食和饮水。所有动物实验均符合四川大学动物保护与伦理委员会的要求,批准号2021164A。

1.2 ZIF-8@Pt的制备和检测

1.2.1 制备

首先合成ZIF-8金属有机框架,将5.65 g 2-甲基咪唑溶解于82 mL去离子水中形成溶液A,再将362 mg Zn(NO₃)₂·6H₂O和10 mg CTAB搅拌溶解于18 mL去离子水中形成溶液B。将上述两种溶液充分混合后在室温下搅拌1 h, 10 000 r/min离心10 min后,收集沉淀,用体积分数50%乙醇洗涤3次。然后将沉淀物在60℃真空烘箱中烘干获得粉末状ZIF-8。随后将54.7 mg的PtCl₄及300 mg干燥后的ZIF-8溶解于25 mL去离子水中,滴加2 mL 1 mol/L的NaBH₄,使混合物反应30 min,离心收集沉淀,体积分数50%乙醇洗涤3次,离心收集后干燥后得到ZIF-8@Pt。

1.2.2 表征

①扫描电镜观察:取少量干燥后的ZIF-8及ZIF-8@Pt,研磨成细粉状,用称量勺蘸取少量于导电胶上。放入扫描电镜(SEM,型号EVO 10,德国ZEISS公司)样品台上,调整聚焦并拍照。②透射电镜观察:分别取1 mg的上述粉末状ZIF-8及ZIF-8@Pt于1.5 mL EP管中,加入1 mL无水乙醇后放入超声清洗仪分散0.5 h。吸取10 μ L于透射电镜载网上,自然晾干后置于透射电镜(TEM,型号JEM-2100 Plus,日本JEOL)样品槽中上机检测。③X-线衍射分析(XRD):将ZIF-8及ZIF-8@Pt压在专用石英板上,置于样品台,设置仪器条件检测后,使用Jade 6软件分析数据,粉末衍射标准联合委员会标准卡比对分析。④X-线电子能谱分析(XPS):将ZIF-8及ZIF-8@Pt压在碳箔上,贴

于样品台上,测试后使用Thermo Advantage分析。

1.2.3 仿酶活性测试

① H₂O₂的清除效率检测:将10 μL的ZIF-8溶液或ZIF-8@Pt溶液(PBS溶解,质量浓度为50 μg/mL)、PBS溶液,分别加到1.97 mL PBS溶液(pH=7.4)中,并加入20 μL H₂O₂(10 mmol/L),混匀后每5 min取50 μL上述液体加入100 μL Ti(SO₄)₂(13.9 mmol/L)中混合,用紫外分光光度计测量在405 nm处的吸光度。过氧化氢含量越多,吸光度值越高。制图时纵坐标为过氧化氢浓度的相对百分比,更为直观地反映过氧化氢的清除。②产O₂性能检测:向20 mL PBS溶液(pH=7.4)中分别加入20 μL的ZIF-8或ZIF-8@Pt溶液(PBS溶解,质量浓度为10 μg/mL)、PBS溶液,溶氧仪确定零氧条件后,再加入0.2 mL H₂O₂(0.1 mol/L),间隔5 s,连续采集70次溶液中的氧气质量浓度。

1.2.4 细胞毒性及体外清除ROS检测

①细胞毒性检测:将RAW264.7细胞接种于96孔板(α-MEM培养基,10%FBS,1×双抗),12 h后按照0、5、10、20、40 μg/mL的浓度梯度加入ZIF-8@Pt。24 h后使用CCK-8试剂检测材料对细胞活性的影响。②细胞观察:将RAW264.7细胞接种于96孔板,12 h后加入LPS(终浓度为500 ng/mL)诱导RAW264.7分化为M1型。更换培养液后,LPS组(作为阳性对照)和ZIF-8@Pt+LPS组(简称ZIF-8@Pt组)分别加入PBS溶液或ZIF-8@Pt溶液(加样后ZIF-8@Pt组终浓度为20 μg/mL),并设置UT组(未特殊处理,不加LPS诱导,放入恒温恒湿孵箱中孵育,作为阴性对照),继续孵育8 h。于倒置显微镜下观察细胞形态并采图。③清除ROS检测:将RAW264.7细胞接种于12孔板,取UT组、LPS组、ZIF-8@Pt组细胞,按照上述处理后,取一部分细胞使用DCFH-DA活性氧检测探针标记RAW264.7细胞内的ROS水平,孵育30 min后采用倒置荧光显微镜观察并采图;取另一部分细胞,流式细胞分析仪检测各组细胞DCFH-DA荧光强度。

1.2.5 ZIF-8@Pt抑制RAW264.7的M1型极化检测

①流式细胞术:CD86及iNOS为M1型巨噬细胞特异标志物,CD206为M2型巨噬细胞特异标志物。通过荧光标记后,经流式细胞分析仪分析各特异性表达细胞群体所占比例。具体为:将3组细胞接种于12孔板并按照上述处理后,吸出培养基,用PBS将细胞轻柔吹下后400 g/5 min离心洗涤,质量分数4%多聚甲醛固定10 min、0.1% Triton透化15 min,加入相应抗体避光孵育30 min后,流式细胞仪检测各组细胞相应的荧光强度。②Western blot检测蛋白表达:将RAW264.7细胞接种到6孔板,UT组放入恒温恒湿孵箱(37 ℃,体积分数5%CO₂)孵育过夜,

LPS组与ZIF-8@Pt组加入LPS刺激,并在低氧孵箱(体积分数:1%O₂、5%CO₂和94%N₂)孵育过夜。提取蛋白后加入loading buffer,混匀后90 ℃、10 min蛋白变性。电泳转膜后,将对应的膜浸于HIF-1α一抗(HIF-1α antibody #3716, CST, 1:1 000)、NF-κB p65一抗(NF-κB p65 rabbit polyclonal antibody, Beyotime, 1:1 000)以及β-actin的一抗(20 536-1-AP, proteintech, 1:1 000)溶液4 ℃过夜孵育。TBST洗涤3次与HRP二抗(SA00001-2, Proteintech, 1:5 000)在室温下摇床孵育1h, TBST洗涤3次后曝光(化学发光成像仪, BIO RAD),蛋白表达量使用ImageJ软件进行条带的灰度值分析。

1.3 体内实验

1.3.1 动物模型构建与给药方法

选用健康成年SD大鼠(7~8周,体质量250~280 g),构建胶原诱导的关节炎模型(collagen-induced arthritis, CIA)。将2 mg/mL的牛Ⅱ型胶原蛋白溶液(CII)与等体积的弗氏不完全佐剂(IFA)在冰浴下经高速剪切机混合、乳化(20 000 r/min, 2 min, 0 ℃冷却5 min),重复2~3次,制成乳剂。于大鼠尾部背侧皮下注射,第1天注射0.2 mL/只进行基础免疫,第7天注射0.1 mL/只加强免疫。每天观察大鼠活动情况及关节处肿胀情况。在初次免疫后的第31天,大鼠已出现跛行,关节明显肿胀、局部皮温升高的症状,视为造模成功。

选取造模成功的大鼠8只随机分为两组:Control组和ZIF-8@Pt组,另取3只未造模鼠作为健康对照组(untreated, UT)。Control组双侧膝关节腔局部注射PBS溶液作为阳性对照,ZIF-8@Pt组双侧膝关节腔局部注射ZIF-8@Pt溶液(质量浓度为2 mg/mL)进行治疗,每次注射50 μL每侧膝关节^[17]。在初次免疫后的第31天、33天、35天、37天及39天共进行5次治疗,第41天处死大鼠,收集大鼠重要脏器、关节和血液样本。

1.3.2 大体观察及影像学评估

大体观察:在造模成功后大鼠每次治疗前和处死前均对大鼠进行大体评估,即在初次免疫后的第31、33、35、37、39和41天,对大鼠进行关节炎评分(0~4分,0分最轻,4分最严重)^[18]、膝关节宽度及体质量的测量,并于处死前进行拍照。针对上述评分,将两名研究人员独立评分后的平均值纳入后续分析。

影像学评估包括高频超声检查及Micro-CT检查。高频超声检查:大鼠处死前一天经小动物超声成像系统来探测关节情况,使用20 MHz高频、“L”型线阵探头,定位至关节水平,聚焦及深度调节至图像清晰,记录编号并存储图像。大鼠关节Micro-CT检查后运用Micro-CT的配

套分析软件(Analyze 12.0, PerkinElmer)对采集的图像的进行三维重建。

1.3.3 大鼠血清及关节炎因子检测

大鼠经异氟烷麻醉后,“V”字形剪开大鼠腹部皮肤,暴露右侧的腹主动脉,在髂总动脉分叉处前方2 mm沿向心端进针,用惰性分离胶促凝管收集血清。血清的炎症指标可以反映RA的全身炎症状态。本研究提取大鼠血清并通过ELISA法对IL-1 β 、C反应蛋白(C-reactive protein, CRP)及TNF- α 等能较好反应全身炎症水平的因子进行检测^[19]。同时对血清进行如谷丙转氨酶(alanine transaminase, ALT)、谷草转氨酶(aspartate aminotransferase, AST)、肌酐(creatinine, Cr)及尿素(urea, UREA)、酪蛋白激酶2(casein kinase 2, CK2)的生化指标检测。处死后取大鼠膝关节,剔除多余组织并匀浆后取上清行TNF- α 、精氨酸酶-1(arginase-1, Arg-1)ELISA检测。

1.3.4 病理学评估

大鼠脏器取出后经制片处理行HE染色观察是否存在脏器损伤。大鼠关节病理染色:大鼠关节取出固定、脱钙、包埋后,制成石蜡切片,进行苏木精-伊红(HE)染色,观察关节炎性细胞浸润及骨质破坏的情况,采用大鼠CIA关节炎病理评分评估严重程度(0~12分,0分最轻,12分最重)^[20]。进行番红O-固绿、TRAP、HIF-1 α 及CD31免疫组织化学染色以及iNOS/CD206多色免疫荧光染色,采用QuPath软件分析阳性细胞百分比。番红O-固绿染色可以观察关节面软骨的破坏程度。TRAP染色可将破骨细胞标记为紫红色,提示破骨活动程度。HIF-1 α 蛋白的阳性率可反映RA大鼠关节腔中缺氧严重程度。CD31免疫组化染色可显示血管内皮细胞的存在,提示血管生成与浸润,可以对RA病理改变中的滑膜血管翳进行验证。采用多重免疫荧光染色对大鼠膝关节滑膜中巨噬细胞标志物的表达情况进行检测,红色荧光代表M1型巨噬细胞标志物iNOS,绿色荧光代表M2型巨噬细胞标志物CD206。

1.4 统计学方法

数据统计分析使用Graphpad Prism 9软件完成,实验数据以 $\bar{x} \pm s$ 表示,各目标参数的多组间比较采用单因素方差分析(ANOVA)进行,然后使用Tukey'法进行P值矫正后的两两比较。 $P < 0.05$ 为差异有统计学意义。

2 结果

2.1 ZIF-8@Pt表征及性能

如图1所示。SEM图像表明ZIF-8及ZIF-8@Pt纳米粒子为标准的立方体纳米框架结构(图1A和图1B)。

TEM图像展示出ZIF-8粒子表面均一,而ZIF-8@Pt纳米粒表面存在对比度较高的颗粒掺杂,提示Pt金属团簇的存在(图1C和图1D)。XPS结果提示ZIF-8@Pt出现Pt的强信号峰,并且以0价态存在(图1E和图1F)。XRD结果中虽未发现明显Pt的晶体峰(图1G),但结合XPS结果中Pt的强信号,考虑Pt的结构不是有晶面的结晶体,而是以团簇形式呈现,这也与TEM中发现的高对比度金属团簇相符。CAT仿酶能力检测发现,ZIF-8@Pt粒子可以高效清除H₂O₂并产生O₂(图1H和图1I),证实其可清除ROS,具备治疗炎症疾病的潜在能力。

2.2 ZIF-8@Pt仿酶纳米制剂体外清除ROS抑制M1型巨噬细胞炎症表达效果

如图2A所示,LPS刺激RAW264.7可诱导其向M1型巨噬细胞分化。如图2B和2C所示,随着ZIF-8或ZIF-8@Pt纳米粒浓度升高,RAW264.7细胞活性出现先升高后降低,差异有统计学意义(与未加入ZIF-8或ZIF-8@Pt时相比, $P < 0.05$)。在20 $\mu\text{g/mL}$ 时,ZIF-8@Pt未表现出明显的细胞毒性,而ZIF-8则将细胞活性抑制至80.0%。因此,后续实验中将ZIF-8@Pt与细胞共孵育的质量浓度设定为20 $\mu\text{g/mL}$ 。光镜观察细胞形态发现(图2D),LPS刺激后RAW264.7细胞出现大量伪足,为M1型巨噬细胞典型特征。而添加ZIF-8@Pt后,细胞伪足明显减少,部分恢复至UT组状态。采用DCFH-DA荧光探针标记细胞内ROS后结果表明(图2D和图2E),LPS诱导大幅提高了RAW264.7细胞内ROS水平(与UT组相比, $P < 0.05$),这一现象同样符合M1型巨噬细胞表现,而ZIF-8@Pt细胞内荧光强度显著下调,证明ZIF-8@Pt可以清除细胞内ROS。而通过流式分析证明(图2E),相较于LPS组,虚线所在位置代表其平均荧光强度,ZIF-8@Pt组荧光峰值左移,提示胞内荧光强度下降,同样验证了ZIF-8@Pt清除细胞内ROS的能力。如图2F和表1所示,iNOS阳性表达细胞群体在经LPS诱导后大幅上升,而在ZIF-8@Pt治疗后显著下降($P < 0.05$)。CD86阳性群体也表现出相似的变化。虽然CD206表达无明显变化,但iNOS⁺/CD206⁺细胞群体比例在经ZIF-8@Pt治疗后有所降低($P < 0.05$),表明巨噬细胞存在向M2型抗炎型巨噬细胞分化的趋势。如图2G和表1所示,与UT组相比,HIF-1 α 以及NF- κB p65的蛋白表达量在LPS组均有所升高($P < 0.05$),而在添加ZIF-8@Pt共培养后,两者表达量均降低(与LPS组相比, $P < 0.05$)。

2.3 ZIF-8@Pt治疗CIA大鼠的大体观察

如图3A可以发现,Control组关节炎程度几乎没有变化,而ZIF-8@Pt组持续走低。治疗过程中UT组体质量

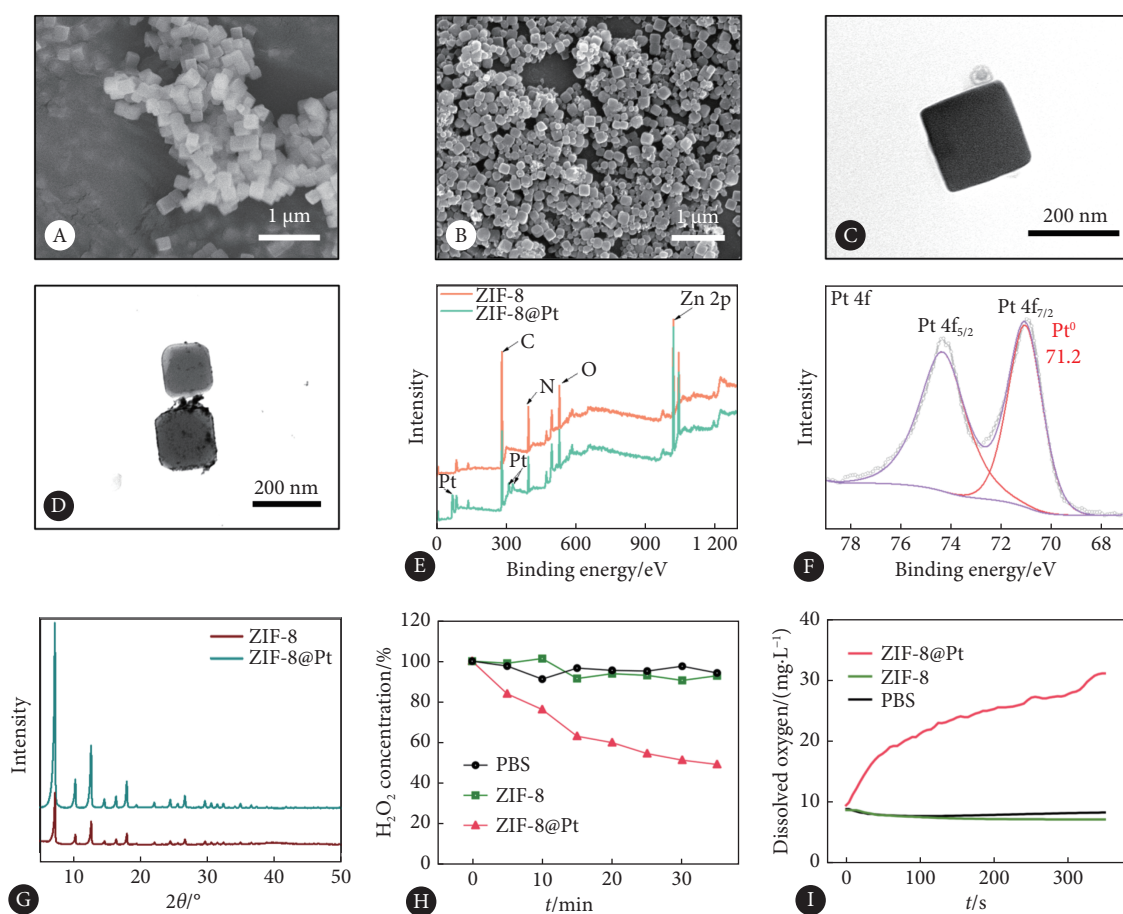


图 1 材料表征及活性氧清除活性

Fig 1 Characterization and ROS-scavenging activity of ZIF-8@Pt

A, SEM image of ZIF-8 nanoparticles; B, SEM image of ZIF-8@Pt nanoparticles; C, TEM image of ZIF-8; D, TEM image of ZIF-8@Pt; E, XPS survey spectra of ZIF-8 and ZIF-8@Pt; F, the Pt 4f XPS analysis of ZIF-8@Pt; G, XRD patterns of ZIF-8 and ZIF-8@Pt; H, H_2O_2 decomposition; I, O_2 production properties of ZIF-8 and ZIF-8@Pt.

最高, 而ZIF-8@Pt组稍高于Control组(图3B), 体质量的下降可能与全身炎症及疼痛导致进食减少有关。双膝关节宽度统计(图3C和图3D)发现ZIF-8@Pt组在治疗后期(第37~41天)关节宽度出现持续下降, 而Control组关节宽度在较高的水平波动。图3E中膝关节的大体观察照片可发现, 对照组膝关节红肿明显, 而ZIF-8@Pt组红肿情况明显减轻, 接近UT组大鼠。

2.4 ZIF-8@Pt治疗大鼠的影像学观察

如图3F中超声图片所示, 正常大鼠膝关节内无异常回声, 关节间隙正常; 而Control组探查至膝关节明显增宽, 可见明显增厚的低回声区, 为增厚的滑膜组织, 此外, 还可见不连续的强回声, 以及关节腔内的数个强回声堆积, 为骨质破坏的表现。而ZIF-8@Pt组的上述表现明显减轻。图3H展示了双膝滑膜厚度统计结果, 证明ZIF-8@Pt的局部注射可以明显缓解关节滑膜肿胀。Micro-CT三维重建结果表明(图3G), 与正常膝关节对比, Control组膝关节出现严重的骨侵蚀及骨赘形成, 几乎不

具备完整关节结构, 而ZIF-8@Pt材料组骨破坏程度明显减轻, 关节骨性结构部分恢复。

2.5 ZIF-8@Pt治疗大鼠的安全性验证

如图4A及表2所示, 与正常大鼠相比较, 各处理组肝肾功能等, 如ALT、AST、Cr、UREA及CK2均未见明显升高。此外, 对大鼠主要脏器的HE染色也可观察到与ZIF-8@Pt组与UT组大鼠脏器细胞形态相比无明显差异, 未见明显损伤, 证明ZIF-8@Pt安全性良好。

2.6 ZIF-8@Pt治疗大鼠的血清及关节炎指标检测

结果如表3所示, Control的炎症反应最严重, 各炎症指标含量显著升高, ZIF-8@Pt组的炎症因子表达量则有所下降($P < 0.05$)。另一方面, 对大鼠的离体关节组织匀浆后经ELISA检测M1及M2型巨噬细胞特异性标志物, Control组M1型巨噬细胞标志物TNF- α 表达量显著升高, 而M2型巨噬细胞标志物Arg-1则有所下降。经ZIF-8@Pt治疗后, TNF- α 显著下调, 并且Arg-1有所回升($P < 0.05$)。

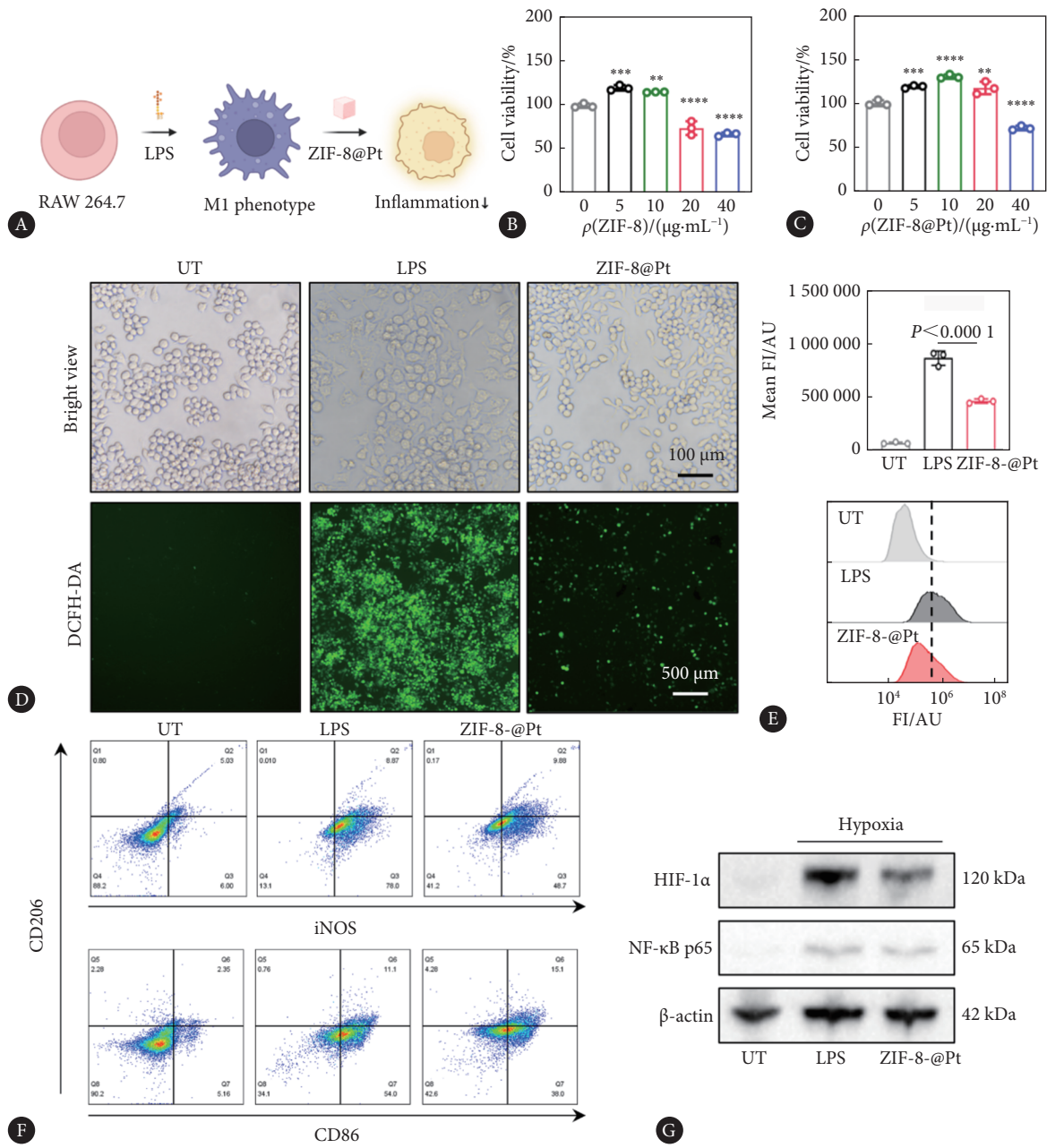


图 2 ZIF-8@Pt生物相容性及清除ROS调节巨噬细胞极化检测

Fig 2 The biocompatibility of ZIF-8@Pt and the effectiveness in intracellular ROS scavenging and regulating macrophage polarization

A, Schematic illustration of the cellular experiment process; B, biocompatibility of ZIF-8 nanoparticles evaluated by CCK-8 assay; C, biocompatibility of ZIF-8@Pt nanoparticles evaluated by CCK-8 assay; D, bright view and fluorescence view of RAW264.7; E, mean FI (top) and flowcytometry analysis of the ROS level (bottom) detected by DCFH-DA (the dashed line indicates the mean FI; FI: fluorescence intensity); F, expression of CD86, CD206, and iNOS by RAW264.7 in different groups detected by flowcytometry; G, Western blot assay revealing the expression levels of HIF-1α, NF-κB, and β-actin. In the above experiment, $n=3$ per group. ** $P<0.01$, *** $P<0.001$, **** $P<0.0001$, vs. 0 $\mu\text{g}/\text{mL}$.

2.7 大鼠关节的病理学评估

本研究对大鼠膝关节进行病理染色检测, 见图5、表4。其中, HE染色发现UT组关节结构清晰, 可见关节软骨及部分滑膜组织。Control组大鼠膝关节滑膜增生严重, 炎性细胞大量浸润, 已不可见正常关节软骨结构。ZIF-8@Pt组滑膜肥厚减轻, 仅有轻微软骨组织破坏, 整体

修复良好。

番红O-固绿的染色结果可见在UT组中, 碱性的番红与嗜碱性的软骨结合呈现红色, 固绿与骨结合呈现蓝绿色, 红色信号完整连续, 表明软骨没有破坏。而Control组可见严重的软骨破坏, 红色信号零星。ZIF-8@Pt治疗后软骨缺失不甚明显, 关节面平整, 软骨较厚, 着色与UT组

表 1 ZIF-8@Pt清除ROS调节巨噬细胞极化检测

Table 1 The effectiveness of ZIF-8@Pt in intracellular ROS scavenging and regulating macrophage polarization

Index	UT group (A)	LPS group (B)	ZIF-8@Pt group (C)	P (A vs. B)	P (A vs. C)	P (B vs. C)
ROS ⁺ live cell/%	4.283±0.875	72.400±3.439	49.700±2.946	<0.000 1	<0.000 1	0.000 2
CD86 positive ratios/%	7.535±0.480	61.305±4.145	55.350±2.340	<0.000 1	<0.000 1	0.033 5
iNOS positive ratios/%	15.470±6.210	75.908±7.811	63.298±3.459	<0.000 1	<0.000 1	0.040 7
iNOS ⁺ /CD206 ⁺ ratios/%	2.145±0.467	8.675±1.108	5.427±0.643	0.000 1	0.005 3	0.005 6
HIF-1α protein relative expression	0.108±0.048	1.154±0.316	0.650±0.054	0.001 2	0.028 1	0.037 5
NF-κB p65 protein relative expression	0.272±0.049	1.144±0.170	0.764±0.174	0.000 7	0.013 4	0.040 3

ROS: reactive oxygen species; CD86: cluster of differentiation 86; iNOS: inducible nitric oxidesynthase; HIF-1α: hypoxia-inducible factor alpha; NF-κB p65: nuclear factor kappa-B p65. In the above groups, $n=3$. The data are presented as $\bar{x} \pm s$.

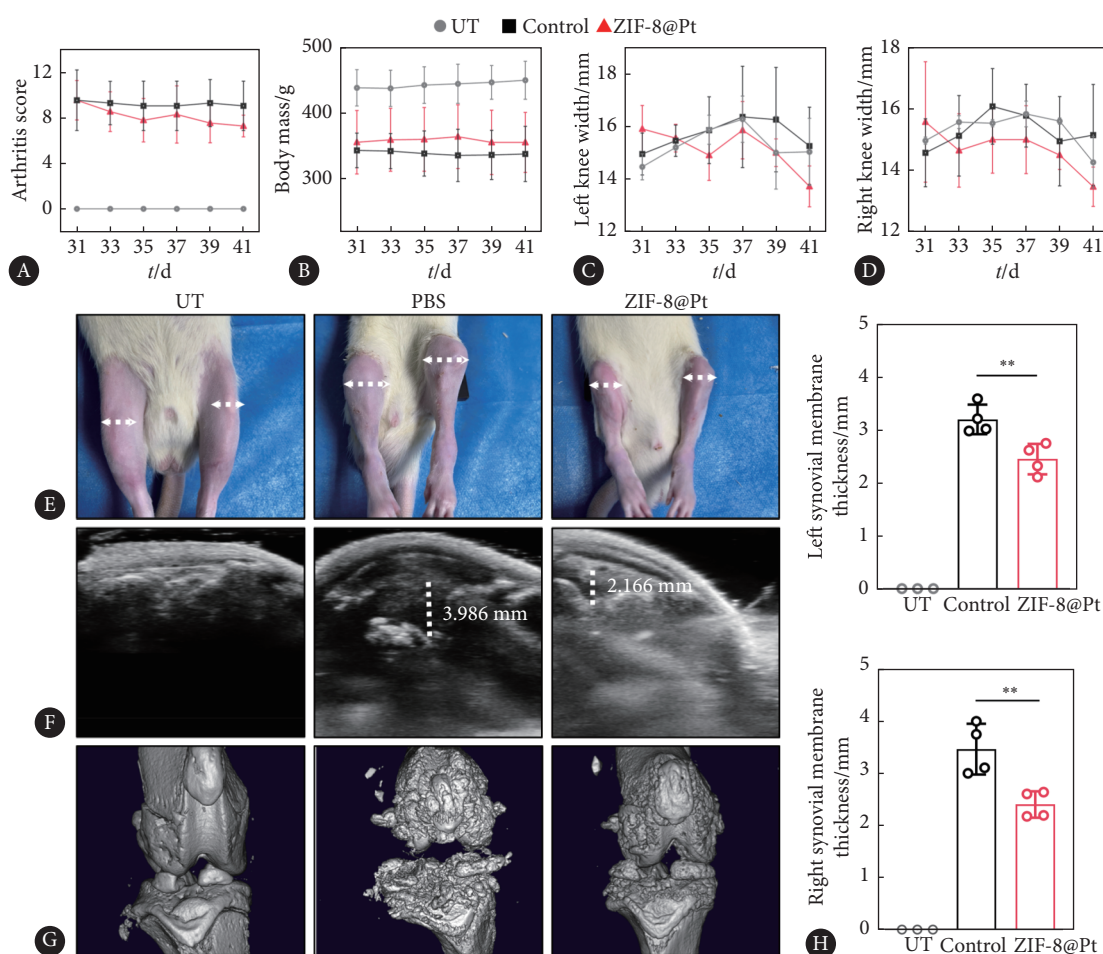


图 3 CIA模型大鼠治疗后的大体及影像学评估

Fig 3 General and imaging evaluations of CIA model rats

A, Arthritis score of the rats; B, body mass change in the rats; C, left knee width of rats in different groups; D, right knee width of rats in different groups; E, visual observation of rats, with the white dotted line indicating the measurement sites; F, B-mode ultrasound evaluation of the synovial membrane; G, 3D-reconstruction of the micro-CT images of rats in different groups; H, left and right synovial membrane thickness assessment of rats in different groups. UT group, $n=3$; Control and ZIF-8@Pt groups, $n=4$. ** $P < 0.01$.

大鼠重合程度较高,提示软骨结构保护良好。

大鼠膝关节TRAP染色后可见,Control组红色区域明显,表明破骨细胞含量极高,破骨代谢旺盛,骨质破坏明

显;而ZIF-8@Pt组较之明显减少,TRAP阳性区域仅在骨髓内少量体现,与UT组较接近,提示ZIF-8@Pt可抑制RA鼠关节的破骨细胞代谢,保护关节骨性结构。

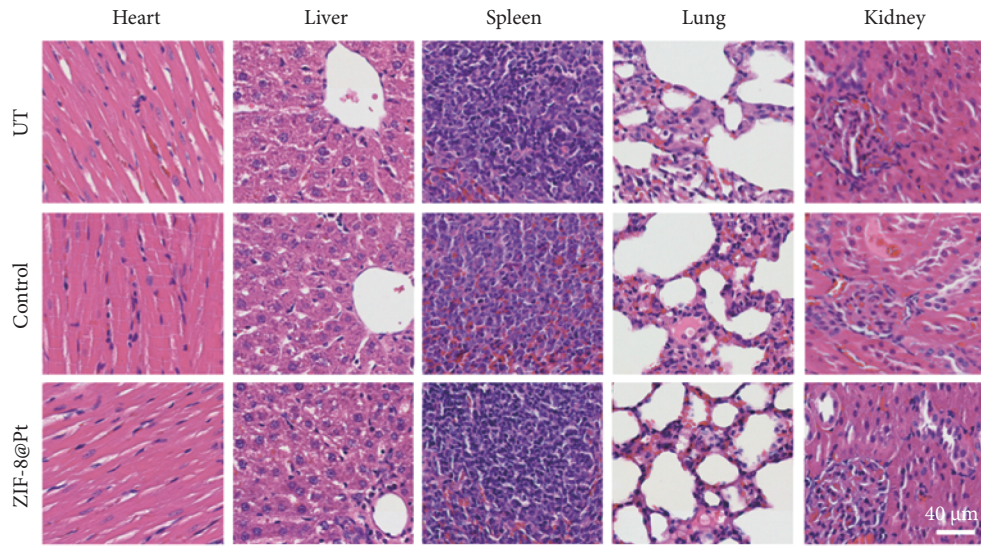


图 4 材料体内安全性验证 (HE染色)

Fig 4 Verification of the *in vivo* biosafety of ZIF-8@Pt (HE staining)

表 2 材料体内安全性

Table 2 Verification of the *in vivo* biosafety of ZIF-8@Pt

Index	UT group (A)	LPS group (B)	ZIF-8@Pt group (C)	<i>P</i> (A vs. B)	<i>P</i> (A vs. C)	<i>P</i> (B vs. C)
ALT/(U/L)	40.333±7.095	32.000±5.944	32.000±4.243	0.1973	0.1973	>0.9999
AST/(U/L)	105.500±7.034	146.950±14.638	143.500±13.990	0.0074	0.0119	0.9248
UREA/(mmol/L)	5.010±0.278	3.713±0.503	4.623±0.621	0.0248	0.5988	0.0810
Cr/(μmol/L)	34.667±6.028	28.750±3.096	22.250±0.500	0.1372	0.0047	0.0761
CK2/(U/L)	1429.000±493.355	1419.250±161.217	1294.750±152.574	0.9989	0.8114	0.8109

ALT: alanine transaminase; AST: aspartate aminotransferase; Cr: creatinine; UREA: urea; CK2: casein kinase 2. UT group, *n*=3; Control and ZIF-8@Pt groups, *n*=4. The data are presented as $\bar{x} \pm s$.

表 3 大鼠血清及膝关节组织炎症因子检测

Table 3 Evaluation of inflammatory factors in the serum and the knee joint

Sample	Index	UT group (A)	LPS group (B)	ZIF-8@Pt group (C)	<i>P</i> (A vs. B)	<i>P</i> (A vs. C)	<i>P</i> (B vs. C)
Serum	IL-1β/(pg/mL)	5.680±0.308	8.838±0.415	7.658±0.315	<0.0001	0.0002	0.0038
	CRP/(ng/mL)	395.663±5.773	554.638±38.314	479.478±31.624	0.0004	0.0173	0.0203
	TNF-α/(pg/mL)	51.060±2.249	75.698±2.728	62.805±1.186	<0.0001	0.0002	<0.0001
Knee joint	Arg-1/(ng/mL)	223.157±10.365	179.668±6.285	215.643±12.129	0.0011	0.5974	0.0022
	TNF-α/(pg/mL)	460.537±32.904	673.050±48.055	565.598±39.832	0.0004	0.0260	0.0159

TNF-α: tumornecrosis factor-α; IL-1β: interleukin-1β; CRP: C-reactive protein; Arg-1: arginase-1. UT group, *n*=3; Control and ZIF-8@Pt groups, *n*=4. The data are presented as $\bar{x} \pm s$.

免疫组织化学染色示, Control组关节中有大量的CD31阳性空腔存在, 表明滑膜血管浸润严重。而ZIF-8@Pt组关节中CD31阳性区域明显减少。Control组滑膜中HIF-1α阳性细胞浸润严重, 而ZIF-8@Pt组阳性率明显下降, 阳性细胞仅部分出现于滑膜组织, 与UT组较接近。这一结果与前述体外实验中ZIF-8@Pt抑制LPS诱导的巨噬细胞内ROS富集, 并抑制HIF-1α表达从而抑制M1型巨噬细胞极化的结果相吻合, 符合ZIF-8@Pt通过仿

酶清除ROS以实现产氧的材料学性能。

多重免疫荧光染色示, Control组内iNOS阳性细胞表达较多, 整体荧光偏红色, 而ZIF-8@Pt组中的绿色荧光表达明显有上升, 与UT组大鼠膝关节的表达相接近。结合前述系列病理学评估可以认为, ZIF-8@Pt可以抑制RA大鼠膝关节巨噬细胞M1型炎性极化, 抑制破骨代谢及滑膜血管新生, 缓解关节局部低氧环境, 最终抑制滑膜增生, 保护关节骨及软骨结构。

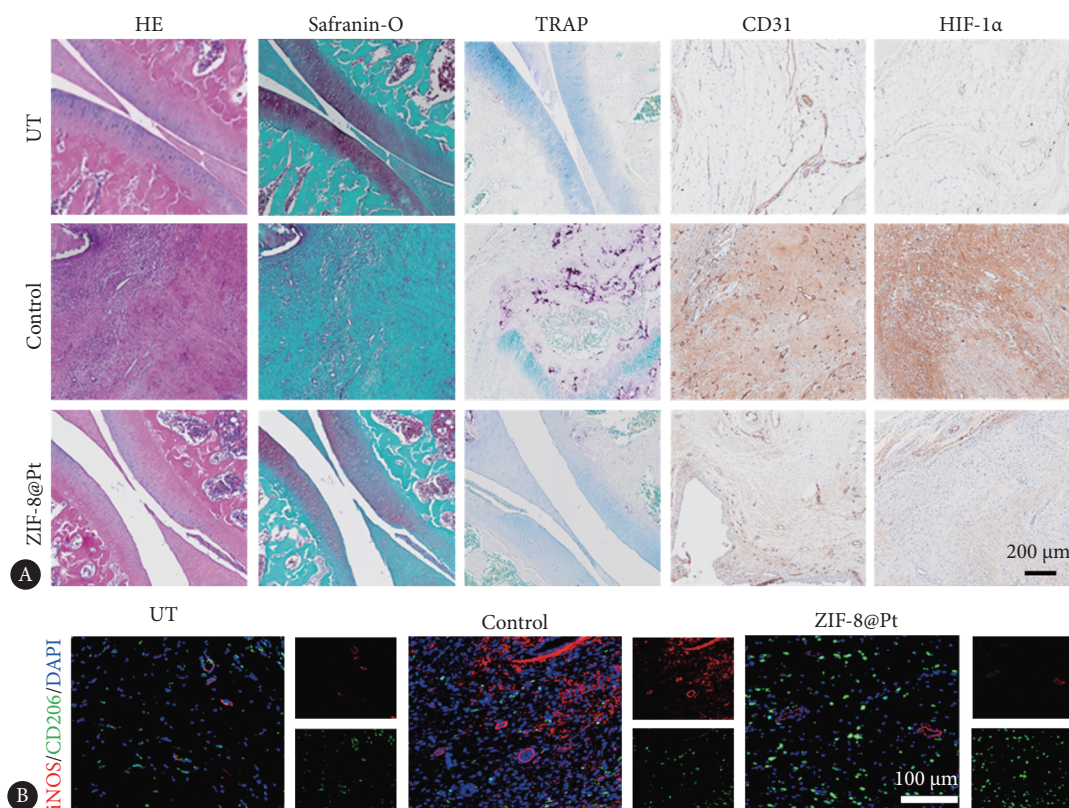


图 5 膝关节组织病理学评估

Fig 5 Histopathological evaluation of the knee joint of rats

A, Representative images of HE staining, Safranin-O staining, TRAP staining, and IHC staining (CD31 antibody and HIF-1 α antibody). B, Representative immunofluorescent images of CD206 (green) and iNOS (red). The nuclei were labelled by DAPI.

表 4 膝关节组织病理学评估

Table 4 Histopathological evaluation of the knee joint of rats

Index	UT group (A)	LPS group (B)	ZIF-8@Pt group (C)	<i>P</i> (A vs. B)	<i>P</i> (A vs. C)	<i>P</i> (B vs. C)
Histology score	0.667 \pm 0.577	10.500 \pm 1.000	8.250 \pm 1.258	<0.000 1	<0.000 1	0.034 9
Trap positive cells/%	2.158 \pm 1.047	57.413 \pm 3.886	11.632 \pm 4.495	<0.000 1	0.023 6	<0.000 1
CD31 positive cells/%	12.113 \pm 2.195	95.016 \pm 3.801	48.441 \pm 9.379	<0.000 1	0.000 2	<0.000 1
HIF-1 α positive cells/%	1.508 \pm 1.281	91.642 \pm 7.731	39.745 \pm 9.213	<0.000 1	0.000 4	<0.000 1
iNOS positive cells/%	12.193 \pm 4.032	85.083 \pm 5.562	26.397 \pm 3.116	<0.000 1	0.007 2	<0.000 1
CD206 positive cells/%	29.162 \pm 5.160	15.101 \pm 4.725	29.848 \pm 6.445	0.025 2	0.985 6	0.013 5

Trap: tartrate-resistant acid phosphase; CD31: platelet endothelial cell adhesion molecule-1; HIF-1 α : hypoxia-inducible factor alpha; iNOS: inducible nitric oxidesynthase; CD206: mannose receptor; UT group, *n*=3; PBS and ZIF-8@Pt groups, *n*=4. The data are presented as $\bar{x} \pm s$.

3 讨论

RA的病理生理机制复杂,而ROS在RA的发生发展中起到关键性的作用。在炎症及自身免疫刺激下导致关节滑膜内ROS激增,促使促炎M1型巨噬细胞数量剧增,而抗炎M2型巨噬细胞减少或处于无活性状态^[21]。紧接着,M1型巨噬细胞进一步合成ROS及分泌多种促炎因子,加重关节炎,形成ROS-炎症的恶性循环^[22-24]。另一方面,ROS的大量合成、滑膜增生及免疫细胞浸润导致关节腔

微环境内耗氧量增加,形成低氧微环境。这将导致关节腔内细胞高表达HIF-1 α ,同时诱导VEGF表达上调,促进滑膜血管内皮细胞增殖,最终导致滑膜血管翳形成^[8]。与此同时,以巨噬细胞为主的免疫细胞产生的促炎细胞因子将刺激滑膜成纤维细胞极化为促炎亚群和组织破坏性亚群,后者可诱导破骨细胞分化,促进骨质破坏并加速软骨的降解^[25]。此外,关节腔内的低氧微环境及高浓度ROS也有利于破骨细胞的分化及生存,这也将加重关节骨质破坏^[26-27]。因此,ROS可作为RA治疗的有效靶点。而

CAT酶(过氧化氢酶)作为调控ROS的重要组成部分,主要可清除H₂O₂并产生氧气^[28],在RA的治疗上有巨大的应用潜能。

既往研究中,多种天然CAT酶被广泛应用于ROS清除的抗炎治疗。如从黑吉豆蛋白质中纯化提取的CAT酶展现出了高效的H₂O₂清除能力^[29];全乳铁蛋白这种天然蛋白质能催化H₂O₂产生氧气缓解肿瘤缺氧微环境^[30];脂质体包封的CAT酶可以催化细胞内源性H₂O₂产生氧气改善组织缺氧^[31];通过富含硼酸的聚合物搭载的超氧化物歧化酶能减少ROS从而恢复视网膜神经节细胞的功能^[32]。然而这些天然成分难制备、难提纯且成本高^[33],因此人造仿酶制剂被大量开发并应用于清除ROS抗炎治疗^[15, 34]。如利用银纳米酶、锰掺杂的可有效生成氧气的纳米酶^[6],都在RA治疗中取得了成功。因此,本研究以ROS为RA的治疗靶点,利用ZIF-8纳米仿酶制剂框架基底,在其上掺杂Pt金属团簇以实现高效仿酶清除ROS以治疗RA。

本研究通过形貌观察、化学结构及成分表征证实了ZIF-8@Pt的金属有有机框架结构及Pt金属团簇的掺杂,并验证了其仿CAT酶能力,可以实现高效清除H₂O₂产生O₂。在体外实验中,证实其无明显细胞毒性,且可有效抑制RAW264.7巨噬细胞内ROS的富集,抑制其向M1型巨噬细胞极化。值得注意的是,低浓度的ZIF-8以及ZIF-8@Pt可以促进RAW267.4细胞的增殖,这可能与细胞的柠檬酸和乳酸的还原过程被抑制,并且嘌呤类化合物增加有关^[35]。通过对HIF-1 α 以及NF- κ B p65蛋白表达量进行分析,提示ZIF-8@Pt可能通过CAT酶活性清除ROS产生O₂,使得HIF-1 α 的含量降低,抑制HIF-1 α /NF- κ B通路来抑制巨噬细胞M1型极化,与既往研究结论相符^[34, 36]。这些实验证实ZIF-8@Pt具备通过抑制胞内ROS富集而抑制巨噬细胞炎症表达的能力,为后续体内抗炎治疗RA打下基础。

在体内实验中,本研究发现ZIF-8@Pt的局部注射可以有效缓解RA所致的大鼠膝关节滑膜增生,降低炎症表达,抑制关节破坏。并且,ZIF-8@Pt可以减少RA大鼠全身及关节局部炎症因子的表达。在大体观察中,膝关节肿胀程度未见明显减轻,这可能与治疗过程中关节肿胀程度的消退较为缓慢,除滑膜之外的组织也存在软组织水肿的问题有关。为了进一步准确评估大鼠关节滑膜肿胀程度,本研究在治疗结束后大鼠处死前使用高频超声评估大鼠的膝关节滑膜炎情况,ZIF-8@Pt治疗后可见膝关节滑膜炎情况明显减轻。ZIF-8@Pt进行膝关节注射后,大鼠体内AST轻度升高,这可能与全身炎症有关^[37]。与此同时,RA全身及关节局部炎症水平在一定程度上表

达降低。在病理染色结果中,本研究证实了ZIF-8@Pt治疗后可抑制滑膜血管翳及关节局部低氧微环境形成,抑制破骨细胞浸润并保护关节骨及软骨结构。此外,关节滑膜处巨噬细胞表型也被ZIF-8@Pt转化为以M2型巨噬细胞为主,抑制了促炎环境的形成。因此,ZIF-8@Pt可以清除ROS作为治疗靶点,安全有效地治疗RA,本研究创新性地证实了ZIF-8@Pt纳米仿酶制剂具备清除ROS治疗RA的效果,这为新型的纳米治疗药物开发及抗炎治疗提供了新的前景。

* * *

作者贡献声明 雷雪兰负责论文构思、初稿写作和审读与编辑写作,邱迺负责论文构思和监督指导,杜方雪负责监督指导和审读与编辑写作。所有作者已经同意将文章提交给本刊,且对将要发表的版本进行最终定稿,并同意对工作的所有方面负责。

Author Contribution LEI Xuelan is responsible for conceptualization, writing--original draft, and writing--review and editing. QIU Li is responsible for conceptualization and supervision. DU Fangxue is responsible for supervision and writing--review and editing. All authors consented to the submission of the article to the Journal. All authors approved the final version to be published and agreed to take responsibility for all aspects of the work.

利益冲突 所有作者均声明不存在利益冲突

Declaration of Conflicting Interests All authors declare no competing interests.

参 考 文 献

- [1] KUROWSKA-STOLARSKA M, ALIVERNINI S. Synovial tissue macrophages in joint homeostasis, rheumatoid arthritis and disease remission. *Nat Rev Rheumatol*, 2022, 18(7): 384–397. doi: 10.1038/s41584-022-00790-8.
- [2] LIU H, ZHU Y, GAO Y, *et al*. NR1D1 modulates synovial inflammation and bone destruction in rheumatoid arthritis. *Cell Death Dis*, 2020, 11(2): 129. doi: 10.1038/s41419-020-2314-6.
- [3] HUMBY F, LEWIS M, RAMAMOORTHY N, *et al*. Synovial cellular and molecular signatures stratify clinical response to csDMARD therapy and predict radiographic progression in early rheumatoid arthritis patients. *Ann Rheum Dis*, 2019, 78(6): 761–772. doi: 10.1136/annrheumdis-2018-214539.
- [4] LI W, SONG Y, LIANG X, *et al*. Mutual-reinforcing sonodynamic therapy against rheumatoid arthritis based on sparfloxacin sonosensitizer doped concave-cubic rhodium nanozyme. *Biomaterials*, 2021, 276: 121063. doi: 10.1016/j.biomaterials.2021.121063.
- [5] CHEUNG E C, VOUSDEN K H. The role of ROS in tumour development and progression. *Nat Rev Cancer*, 2022, 22(5): 280–297. doi: 10.1038/s41568-021-00435-0.
- [6] HERB M, SCHRAMM M. Functions of ROS in macrophages and

- antimicrobial immunity. *Antioxidants (Basel)*, 2021, 10(2): 313. doi: 10.3390/antiox10020313.
- [7] JOSHI-BARR S, De GRACIA LUX C, MAHMOUD E, *et al.* Exploiting oxidative microenvironments in the body as triggers for drug delivery systems. *Antioxid Redox Signal*, 2014, 21(5): 730–754. doi: 10.1089/ars.2013.5754.
- [8] SHANG Z Z, QIN D Y, LI Q M, *et al.* Dendrobium huoshanense stem polysaccharide ameliorates rheumatoid arthritis in mice via inhibition of inflammatory signaling pathways. *Carbohydr Polym*, 2021, 258: 117657. doi: 10.1016/j.carbpol.2021.117657.
- [9] BARTOK B, FIRESTEIN G S. Fibroblast-like synoviocytes: key effector cells in rheumatoid arthritis. *Immunol Rev*, 2010, 233(1): 233–255. doi: 10.1111/j.0105-2896.2009.00859.x.
- [10] YANG Y, GUO L, WANG Z, *et al.* Targeted silver nanoparticles for rheumatoid arthritis therapy via macrophage apoptosis and re-polarization. *Biomaterials*, 2021, 264: 120390. doi: 10.1016/j.biomaterials.2020.120390.
- [11] TANG Q, CUI J, TIAN Z, *et al.* Oxygen and indocyanine green loaded phase-transition nanoparticle-mediated photo-sonodynamic cytotoxic effects on rheumatoid arthritis fibroblast-like synoviocytes. *Int J Nanomedicine*, 2017, 12: 381–393. doi: 10.2147/IJN.S120902.
- [12] RENDRA E, RIABOV V, MOSSEL D M. Reactive oxygen species (ROS) in macrophage activation and function in diabetes. *Immunobiology*, 2019, 224(2): 242–253. doi: 10.1016/j.imbio.2018.11.010.
- [13] CHAUHAN K, JANDU J S, BRENT L H, *et al.* *Rheumatoid Arthritis*. StatPearls. Treasure Island (FL): StatPearls Publishing, 2024.
- [14] LI X, WANG H, ZOU X, *et al.* Methotrexate-loaded folic acid of solid-phase synthesis conjugated gold nanoparticles targeted treatment for rheumatoid arthritis. *Eur J Pharm Sci*, 2022, 170: 106101. doi: 10.1016/j.ejps.2021.106101.
- [15] XU D, WU L, YAO H, *et al.* Catalase-like nanozymes: classification, catalytic mechanisms, and their applications. *Small*, 2022, 18(37): 2203400. doi: 10.1002/smll.202203400.
- [16] KIM J, KIM H Y, SONG S Y, *et al.* Synergistic oxygen generation and reactive oxygen species scavenging by manganese ferrite/ceria co-decorated nanoparticles for rheumatoid arthritis treatment. *ACS Nano*, 2019, 13(3): 3206–3217. doi: 10.1021/acsnano.8b08785.
- [17] TAMURA T, HIGUCHI Y, KITAMURA H, *et al.* Novel hyaluronic acid-methotrexate conjugate suppresses joint inflammation in the rat knee: efficacy and safety evaluation in two rat arthritis models. *Arthritis Res Ther*, 2016, 18(1): 79. doi: 10.1186/s13075-016-0971-8.
- [18] LU Y, STINETTE T W, WESTRICK E, *et al.* Treatment of experimental adjuvant arthritis with a novel folate receptor-targeted folic acid-aminopterin conjugate. *Arthritis Res Ther*, 2011, 13(2): R56. doi: 10.1186/ar3304.
- [19] WANG L, ZHU B, HUANG J, *et al.* Ultrasound-targeted microbubble destruction augmented synergistic therapy of rheumatoid arthritis via targeted liposomes. *J Mater Chem B*, 2020, 8(24): 5245–5256. doi: 10.1039/D0TB00430H.
- [20] ZHU W, SUN X, ZHU L, *et al.* A novel BlyS peptibody down-regulates b cell and t helper cell subsets *in vivo* and ameliorates collagen-induced arthritis. *Inflammation*, 2016, 39(2): 839–848. doi: 10.1007/s10753-016-0314-6.
- [21] ROSS E A, DEVITT A, JOHNSON J R. Macrophages: the good, the bad, and the gluttony. *Front Immunol*, 2021, 12. doi: 10.3389/fimmu.2021.708186.
- [22] CUTOLO M, CAMPITIELLO R, GOTELLI E, *et al.* The role of M1/M2 macrophage polarization in rheumatoid arthritis synovitis. *Front Immunol*, 2022, 13: 867260. doi:10.3389/fimmu.2022.867260.
- [23] MCINNES I B, SCHETT G. Pathogenetic insights from the treatment of rheumatoid arthritis. *Lancet*, 2017, 389(10086): 2328–2337. doi: 10.1016/S0140-6736(17)31472-1.
- [24] HOSHINO-NEGISHI K, OHKURO M, NAKATANI T, *et al.* Role of anti-fractalkine antibody in suppression of joint destruction by inhibiting migration of osteoclast precursors to the synovium in experimental arthritis. *Arthritis Rheumatol*, 2019, 71(2): 222–231. doi: 10.1002/art.40688.
- [25] KOMATSU N, TAKAYANAGI H. Mechanisms of joint destruction in rheumatoid arthritis-immune cell-fibroblast-bone interactions. *Nat Rev Rheumatol*, 2022, 18(7): 415–429. doi: 10.1038/s41584-022-00793-5.
- [26] MURATA K, FANG C, TERAOKA C. Hypoxia-sensitive COMMD1 integrates signaling and cellular metabolism in human macrophages and suppresses osteoclastogenesis. *Immunity*, 2017, 47(1): 66–79. e5. doi:10.1016/j.immuni.2017.06.018.
- [27] DOI K, MURATA K, ITO S, *et al.* Role of lysine-specific demethylase 1 in metabolically integrating osteoclast differentiation and inflammatory bone resorption through hypoxia-inducible factor 1 α and E2F1. *Arthritis Rheumatol*, 2022, 74(6): 948–960. doi: 10.1002/art.42074.
- [28] LIU H, LI Y, SUN S, *et al.* Catalytically potent and selective clusterzymes for modulation of neuroinflammation through single-atom substitutions. *Nat Commun*, 2021, 12(1): 114. doi: 10.1038/s41467-020-20275-0.
- [29] KANDUKURI S S, NOOR A, RANJINI S S, *et al.* Purification and characterization of catalase from sprouted black gram (*Vigna mungo*) seeds. *J Chromatogr B Analyt Technol Biomed Life Sci*, 2012, 889–890: 50–54. doi: 10.1016/j.jchromb.2012.01.029.
- [30] ZHANG Z, YANG J, MIN Q, *et al.* Holo-lactoferrin modified liposome for relieving tumor hypoxia and enhancing radiochemotherapy of cancer. *Small*, 2019, 15(6): 1803703. doi: 10.1002/smll.201803703.
- [31] SHI C, LI M, ZHANG Z, *et al.* Catalase-based liposomal for reversing immunosuppressive tumor microenvironment and enhanced cancer chemo-photodynamic therapy. *Biomaterials*, 2020, 233: 119755. doi: 10.1016/j.biomaterials.2020.119755.
- [32] ZHOU X, LV J, LI G, *et al.* Rescue the retina after the ischemic injury by polymer-mediated intracellular superoxide dismutase delivery.

- Biomaterials, 2021, 268: 120600. doi: 10.1016/j.biomaterials.2020.120600.
- [33] XIANG K, WU H, LIU Y, *et al.* MOF-derived bimetallic nanozyme to catalyze ROS scavenging for protection of myocardial injury. *Theranostics*, 2023, 13(8): 2721–2733. doi: 10.7150/thno.83543.
- [34] LI Y, LIANG Q, ZHOU L, *et al.* An ROS-responsive artesunate prodrug nanosystem co-delivers dexamethasone for rheumatoid arthritis treatment through the HIF-1 α /NF- κ B cascade regulation of ROS scavenging and macrophage repolarization. *Acta Biomater*, 2022, 152: 406–424. doi: 10.1016/j.actbio.2022.08.054.
- [35] LI N, DU Q, JING Z, *et al.* Study of the effects of Au@ZIF-8 on metabolism in mouse RAW 264.7 macrophages. *Biomater Adv*, 2022, 138: 212800. doi: 10.1016/j.bioadv.2022.212800.
- [36] KHOJAH H M, AHMED S, ABDEL-RAHMAN M S, *et al.* Reactive oxygen and nitrogen species in patients with rheumatoid arthritis as potential biomarkers for disease activity and the role of antioxidants. *Free Radic Biol Med*, 2016, 97: 285–291. doi: 10.1016/j.freeradbiomed.2016.06.020.
- [37] LU J, WANG M, CHEN Y, *et al.* NAMPT inhibition reduces macrophage inflammation through the NAD⁺/PARP1 pathway to attenuate liver ischemia-reperfusion injury. *Chem Biol Interact*, 2023, 369: 110294. doi: 10.1016/j.cbi.2022.110294.

(2024-02-01收稿, 2024-07-05修回)

编辑 吕熙



开放获取 本文使用遵循知识共享署名—非商业性使用4.0国际许可协议 (CC BY-NC 4.0), 详细信息请访问

<https://creativecommons.org/licenses/by/4.0/>。

OPEN ACCESS This article is licensed for use under Creative Commons Attribution-NonCommercial 4.0 International license (CC BY-NC 4.0). For more information, visit <https://creativecommons.org/licenses/by/4.0/>.

© 2024 《四川大学学报(医学版)》编辑部 版权所有

Editorial Office of *Journal of Sichuan University (Medical Science)*